Available online at www.sciencedirect.com
ScienceDirect
Nuclear Physics B Proceedings Supplement 00 (2012) 1–12
Nuclear Physics B Proceedings Supplement

Recent results on generalized parton distributions from the COMPASS, HERMES, and Jefferson Lab's Hall A and CLAS Collaborations

Gunar Schnell

Department of Theoretical Physics, University of the Basque Country UPV/EHU, 48080 Bilbao, Spain and IKERBASQUE, Basque Foundation for Science, 48011 Bilbao, Spain

Abstract

Experimental results from COMPASS, HERMES, and Jefferson Lab on generalized parton distributions are reviewed. Two phenomenological approaches to extractions of generalized parton distributions are presented and a short outlook to future measurements is given.

Keywords: generalized parton distributions, nucleon tomography, exclusive reactions, deep-inelastic scattering

1. Introduction

In the past decade the exploration of the three-dimensional structure of hadrons and hadronization has greatly gained in attention. This is partly due, on the one side, to the necessity of going beyond the approximation of collinear moving partons, i.e., using transverse-momentum-dependent parton distributions (TMDs) in the description of nucleon structure, for the description of, e.g., various (transverse) spin effects; and, on the other side, the establishment of the relation between moments of generalized parton distributions (GPDs) and the angular-momentum decomposition of the proton structure. Both, TMDs and GPDs, can be inferred from Wigner distributions that correlate spin, momentum and position space.

While TMDs provide correlated information on the momentum components of partons as well as their and the nucleon's spin, GPDs correlate the spins, the transverse position of partons and their longitudinal momentum [1, 2, 3, 4, 5, 6, 7, 8, 9]. Generalized parton distributions can thus be interpreted as longitudinal-momentum-fraction dissected and quark-flavor separated form factors.

Information about GPDs can be obtained from various experimental observables. One of the theoretically cleanest channels is deeply virtual Compton scattering, DVCS, the hard exclusive lepto-production of real photons. Figure 1 (a) shows a schematic diagram of DVCS, which factorizes in hard scattering parts and the soft part parametrized in terms of GPDs, describing the nucleon [10]. Figure 1 (b) illustrates the Bethe–Heitler process, in which the photon is emitted by the lepton.

Both processes, DVCS and Bethe–Heitler, are experimentally indistinguishable from from each other. The squared amplitude relevant for the cross section for exclusive lepto-production of real photons thus receives contributions from the squared DVCS amplitude $\mathcal{T}_{\mathrm{DVCS}}$, the squared Bethe–Heitler amplitude $\mathcal{T}_{\mathrm{BH}}$, and the interference of both the DVCS and Bethe–Heitler processes:

$$\begin{aligned} |\mathcal{T}|^2 &= |\mathcal{T}_{\mathrm{BH}} + \mathcal{T}_{\mathrm{DVCS}}|^2 \\ &= |\mathcal{T}_{\mathrm{BH}}|^2 + |\mathcal{T}_{\mathrm{DVCS}}|^2 + \underbrace{\mathcal{T}_{\mathrm{DVCS}}\,\mathcal{T}^{*}_{\mathrm{BH}} + \mathcal{T}^{*}_{\mathrm{DVCS}}\,\mathcal{T}_{\mathrm{BH}}}_{\mathrm{I}} \,. \end{aligned}$$

In particular, the interference term I plays an important role at current fixed-target experiments, in which the Bethe–Heitler cross section dominates over the DVCS cross section, as the DVCS amplitude gets enhanced by the large Bethe–Heitler amplitude. The interference of both processes gives thus the chance to study GPDs even in a situation when DVCS as a process itself is suppressed. Moreover, while the DVCS cross section is bilinear in GPDs the interference term is linear [11].

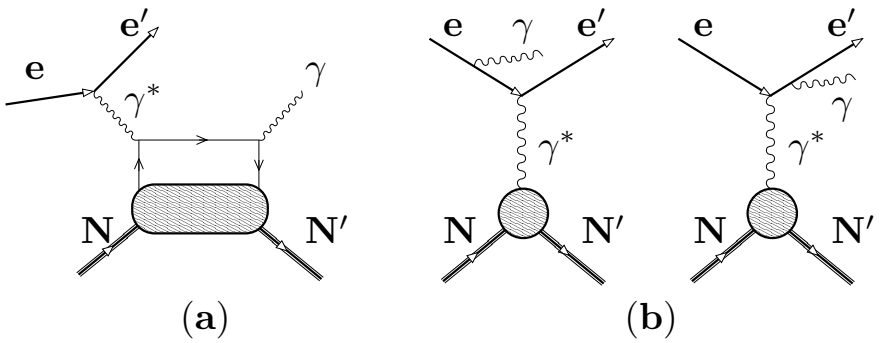

Figure 1: Leading order diagrams for DVCS (a) and Bethe–Heitler (b) processes.

Besides exclusive production of real photons, exclusive production of mesons (Fig. 2) can be used to constrain GPDs. The possibility to investigate GPDs in meson production relies on factorization theorems proven in the framework of pQCD for hard production of mesons by longitudinal virtual photons. Meson production can be factorized in a hard-scattering part and a soft part that depends on the structure of the nucleon and the produced meson [12, 13]. In the case of exclusive vector-meson production, also the produced meson has to be longitudinally polarized.

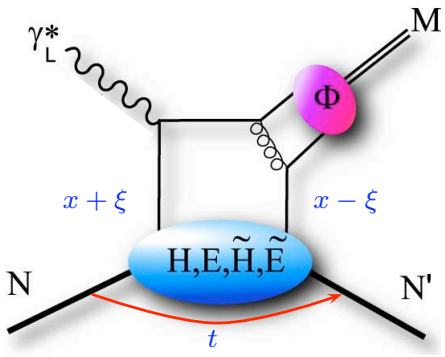

Figure 2: Schematic presentation of exclusive meson production. The quantum numbers of the final-state meson M determine the sensitivity to the various GPDs.

In general, the quantum numbers of the produced particle (real photon vs. vector- or pseudo-scalar meson) determine the sensitivity to the various GPDs. At leading twist and without parton-helicity flip, four types of GPDs are needed to describe the nucleon structure (in general, the partonic structure of any spin-1/2 hadron): $H^{q,g}$, $E^{q,g}$, $\widetilde{H}^{q,g}$, and $\widetilde{E}^{q,g}$, where q stands for a quark flavour and g for a gluon. The GPDs are functions of t, x, and ξ, where t is the squared four-momentum transfer to the nucleon, x the average, and ξ half the difference of the longitudinal momentum fractions of the quark or gluon in the initial and final state. Deeply virtual Compton scattering is sensitive to all four types of quark GPDs, while exclusive lepto-production of pseudo-scalar mesons mainly probe $\widetilde{H}^q$ and $\widetilde{E}^q$, and production of vector-mesons depends mainly on the GPDs $H^{q,g}$ and $E^{q,g}$. The choice of meson also affects the parton-flavor combination probed, e.g., while ρ^0 production is mainly sensitive to the quark-flavor combination $2u + d$ (as well as to gluons), ρ^+ production is sensitive to the difference $u - d$.

The GPDs $H^{q,g}$ and $E^{q,g}$ are of particular interest. Their first (second) x-moments were found to relate directly to the total angular momenta carried by the gluons (quarks) in the nucleon via the *Ji relation* [4]. This finding offers a path towards solving the infamous "nucleon-spin puzzle" of how the helicities and orbital angular momenta of quarks and gluons combine to form the spin of the nucleon. Furthermore, nucleon elastic form factors and ordinary PDFs appear as x-moments of GPDs and kinematic limits ($t \to 0$), respectively.

2. Azimuthal asymmetries

Most results are obtained on the Fourier expansion in the angle ϕ between the photon- or meson-production plane, respectively, and the lepton-scattering plane about the direction of the virtual photon exchanged; as well as in the angle ϕ_S between the target-spin vector and the lepton-scattering plane in case of transverse target polarization. An illustration of the angles for the case of real-photon production (likewise meson production with the momentum of the photon replaced by the one of the meson produced) is given in Fig. 3, in accordance with the *Trento Conventions* [14].

In particular, a wealth of data on single- and double-spin asymmetries (in both the beam and target polarization) are available, among others because many experimental uncertainties are minimized in spin asym-

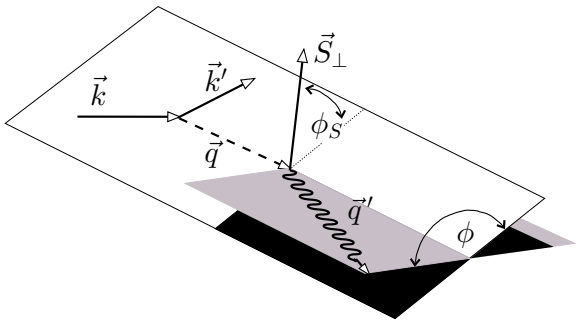

Figure 3: Illustration of the azimuthal angles for exclusive lepto-production of photons in the target rest frame. The lepton-scattering plane is defined by the three-momenta $\vec{k}$ and $\vec{k}'$ of the incoming and outgoing lepton and the photon-production plane correspondingly by $\vec{q} = \vec{k} - \vec{k}'$ and the momentum $\vec{q}\,'$ of the real photon. The angle ϕ_S is between the lepton-scattering plane and $\vec{S}_\perp$, the component of the target polarisation vector that is orthogonal to $\vec{q}$.

metries. Moreover, spin asymmetries are especially interesting as the various beam and target polarizations provide information on different types of GPDs. Especially transverse target-spin asymmetries in vector-meson and in real-photon production on a proton target give the rare opportunity to study the GPD E needed for the Ji relation. Last but not least, beam-charge asymmetries can be studied in lepto-production of real-photons, for which the interference term is sensitive to the charge of the beam lepton. This beam-charge dependence can thus be utilized to separate contributions stemming from the squared DVCS amplitude from the ones of the DVCS/Bethe–Heitler interference.

3. Experiments

Fixed-target experiments from three deep-inelastic-scattering facilities are considered here: COMPASS at CERN, HERMES at DESY, and CLAS and the Hall A Collaboration at Jefferson Lab. Each of them has its own peculiarities.

All lepton beams involved are longitudinally polarized. While the experiments at Jefferson Lab and DESY use electrons (and also positrons in case of the latter), COMPASS at CERN uses highly polarized muons from pion decays. This correlates the helicity of the beam with the beam charge. Only at HERMES the combination of beam charge and helicity is unconstrained.

Luminosity is highest at Jefferson Lab. Luminosity at HERMES is constrained by the beam life-time contribution of the target gas internal to the lepton beam line. At COMPASS the beam intensity is naturally smaller, which is compensated by the target density.

All but the Hall A Collaborations use a large-acceptance spectrometer, approaching nearly full coverage at CLAS. This is relevant when measuring correlated kinematic dependences.

So far, only HERMES had the flexibility in choosing a wide range of pure nucleon and nuclear targets. In particular when target polarization is involved, all other experiments (except for results on polarized helium at Jefferson Lab) use nuclear, e.g., ammonium, targets. Longitudinal target polarization was employed at all three laboratories, while transverse target polarization was available for exclusive reactions only at COMPASS and HERMES, but is planned also for the Jefferson Lab experiments.

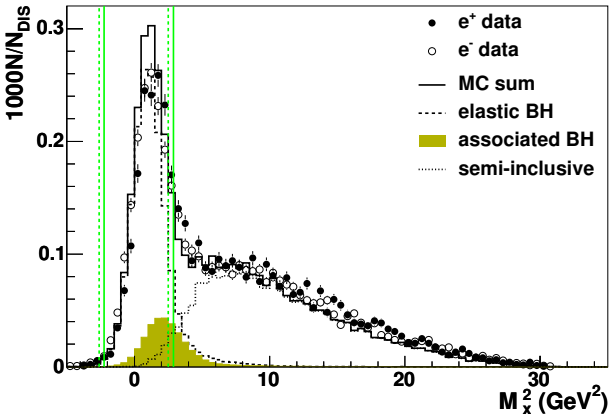

Figure 4: Example distributions (HERMES) in squared missing-mass from data with positron (filled points) and electron (empty circles) beams and from Monte Carlo simulations (solid line). The latter include elastic Bethe–Heitler (dashed line) and associated Beithe–Heitler (filled area) processes as well as semi-inclusive background (dotted line). The simulations and data are both absolutely normalized. The vertical solid (dashed) lines enclose the selected exclusive region for the positron (electron) data.

Most results rely on the missing-mass technique, i.e., the recoiling nucleon is not detected, to select exclusive events (cf. Fig. 4 and discussion in Sec. 4). In particular at higher beam energies the resolution in the missing mass is often not good enough to ensure a clean event sample, which leads to background contributions from both semi-inclusive events but also from processes in which the target nucleon is excited to a higher-mass resonance. Only recently, the HERMES experiment reported first preliminary results for pure DVCS, employing the recoil-proton detector that was used during the last two data-taking years.

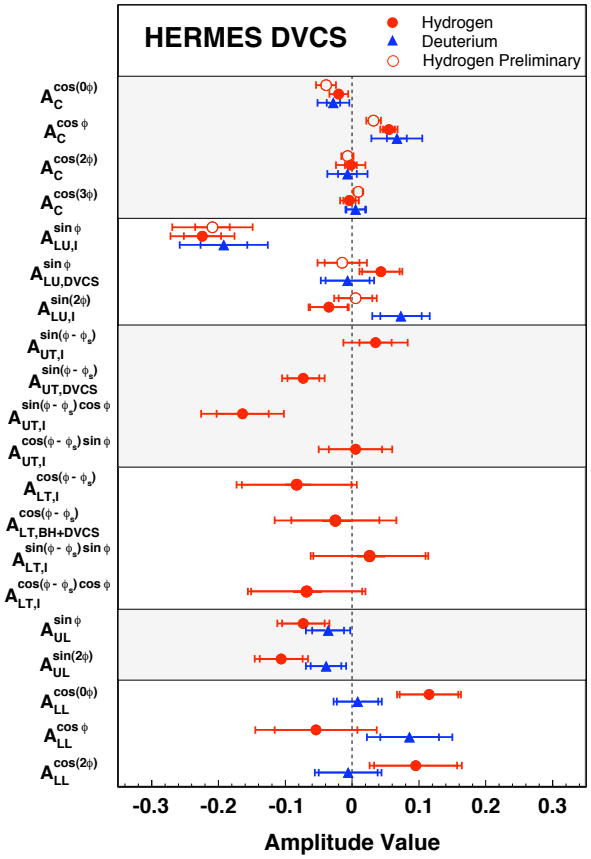

Figure 5: Overview of Fourier amplitudes of various asymmetries in exclusive lepto-production of real photons from the HERMES Collaboration. The various categories from top to bottom: beam-charge asymmetry, beam-helicity asymmetry, transverse target-spin asymmetry, and longitudinal target-spin asymmetry (in the latter two cases both single- and double-spin asymmetries). Inner error bars are statistical uncertainties only, while the outer ones are statistical and systematic uncertainties added in quadrature.

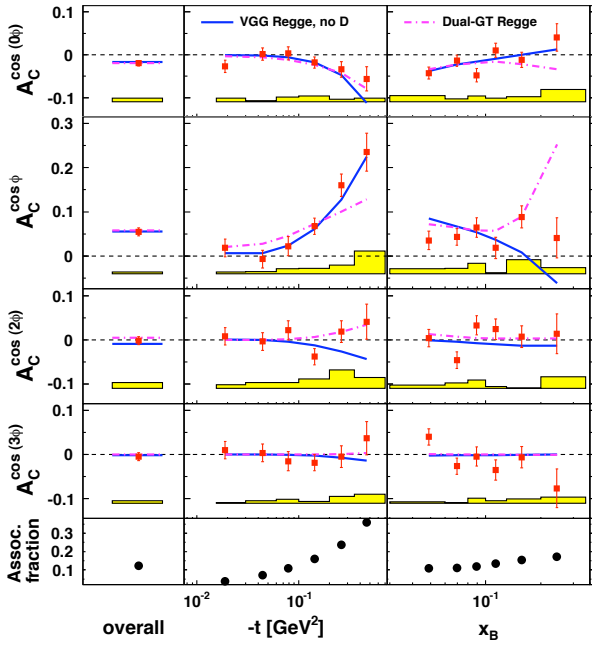

Figure 6: Kinematic dependences of Fourier amplitudes of the beam-charge asymmetry measured by the HERMES Collaboration. In the top two rows the leading amplitudes sensitive to GPD H are shown. The $\cos 2\phi$ amplitude is a higher-twist contribution and the $\cos 3\phi$ is sensitive to gluon GPDs.

4. Results

Up-to-now the experiments at Jefferson Lab as well as the HERMES Collaboration at DESY have presented results on DVCS.[1] The COMPASS experiment at CERN has only performed feasibility studies for their ambitious future GPD program. All experiments have reported results on exclusive meson production.

4.1. Exclusive production of real photons

Deeply virtual Compton scattering is the most favorable channel at present to access GPDs. A decade ago pioneering results on the beam-spin asymmetry were reported by CLAS [15] and HERMES [16]. Since then, precision has improved vastly and the variety of observables has increased.

The most complete set of DVCS observables comes from the HERMES Collaboration. In Fig. 5 an overview of various Fourier amplitudes of the beam-charge ("A_C"), beam-helicity ("A_{LU}"), transverse ("A_{UT}" and "A_{LT}") and longitudinal ("A_{UL}" and "A_{LL}") target-spin asymmetries (both single-(target-)spin and double-spin asymmetries) in exclusive lepto-production of real photons are presented [17, 18, 19, 20, 21, 22]. The Fourier amplitudes are integrated over the kinematic range accepted by the experiment and given for both hydrogen and deuterium targets where applicable. Due to the availability of both beam charges, a separation of contributions from the squared DVCS amplitude and from the DVCS and Bethe–Heitler interference is possible at HERMES. This is indicated by the additional subscripts "DVCS" and "I" when such separation was performed. Details about the extraction technique can be found, e.g., in Ref. [19].

The various asymmetries exhibit differing sensitivities to the various GPDs [11]. Both the constant term and the $\cos\phi$ amplitudes of the beam-charge as well

[1] The *ep* collider experiments are not subject of this review.

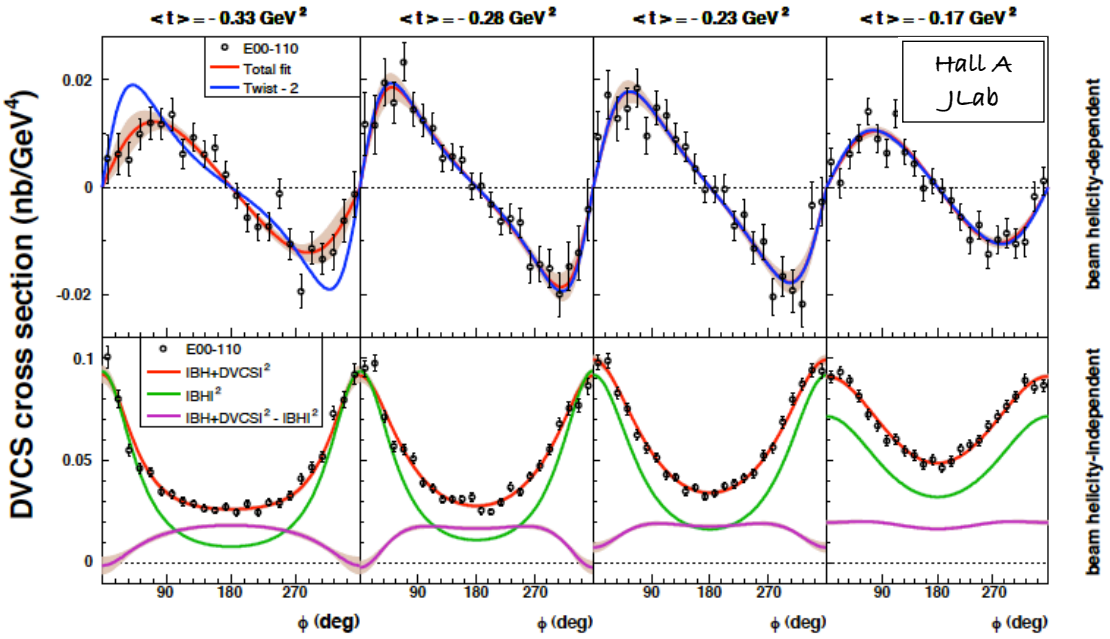

Figure 7: Jefferson Lab Hall A Collaboration results on the cross section for exclusive lepto-production of real photons, beam-helicity dependent (top) and averaged over beam polarization (bottom). Shown is the ϕ dependence in several bins of t of data. Overlaid are in the top panels fits to the data including the leading-twist dependence only as well as including all azimuthal dependences. Only the latter succeeds in describing the data satisfactory in all t bins. In the bottom the contribution from Bethe–Heitler only and the sum (on the amplitude level) of Bethe–Heitler and DVCS are superimposed on the data, with the difference of the two curves plotted as well in the bottom part of the panels.

as the $\sin\phi$ amplitude of the beam-helicity asymmetries are mainly sensitive to the GPD H. However, in case of the beam-charge asymmetry the amplitudes relate to the real part of the Compton form factor —a convolution of GPDs with hard scattering kernels— involving H, while the beam-helicity asymmetry relates to the imaginary part. In praxis this results in a sensitivity to H along the diagonal $x = \xi$ for the beam-helicity asymmetry and to the x-integral of H for the beam-charge asymmetry.

These three Fourier amplitudes are significantly non-zero, with the $sin\phi$ amplitude of the beam-helicity asymmetry being the largest amplitude measured in connection with DVCS. Also apparent is the anticipated sign change and enhancement of the amplitudes going from the constant term to the $\cos\phi$ amplitudes of the beam-charge asymmetry. This can be seen in more detail in Fig. 6 where the t and x_B dependences are shown and compared to two model calculations.

So far, only HERMES has published results on the beam-charge asymmetry. The same holds for the transverse (target) spin asymmetries. The latter give the rare opportunity to study the GPD E. In particular, the $\sin(\phi - \phi_S)$ amplitudes have been shown to be sensitive to the angular momentum carried by quarks and were used, in a very model-dependent way, in constraints on the angular-momentum contributions of u and d quarks to the nucleon spin [19].

The amplitudes of the longitudinal target-spin asymmetries are mainly influenced by the GPD $\widetilde{H}$. This might not come as a surprise, as the forward limit of $\widetilde{H}$ is the quark-helicity distribution also governing longitudinal spin asymmetries in inclusive and semi-inclusive DIS. While the leading amplitudes of the single-spin asymmetries turn out to be negative, the amplitudes of the double-spin asymmetries tend toward positive values.

The impressive power of large luminosities can be observed in the results on the beam-helicity dependent and independent cross-section measurements at Jefferson Lab. Figure 7 shows the ϕ dependences of the beam-helicity dependent cross section and the polarization-averaged one from the Hall A Collaboration [23]. Using ^{3}He as a quasi-neutron target [24], the beam-helicity asymmetry can also be used to constrain the GPD E whose contribution is not suppressed as much for neutron targets compared to proton targets. Thus model-dependent constraints on the angular momentum of quarks can be derived, similarly to what was done for the transverse target-spin asymmetries at HERMES. This is demonstrated in Fig. 8 where two model calcu-

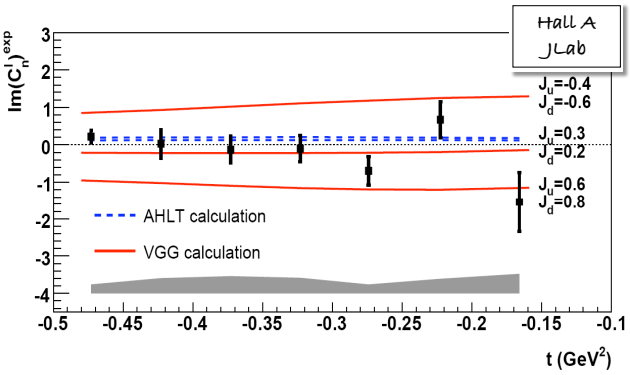

Figure 8: The t-dependence of the extracted incoherent n-DVCS contribution to the beam-helicity asymmetry on a ^{3}He target at the Jefferson Lab Hall A experiment [24]. Solid lines demonstrate the sensitivity to the angular momenta of valence quarks and thus to the GPD E in the framework of the VGG model [25].

lations [25, 26] based on differing assumptions on the angular momenta of quarks are compared to data for the Compton form factor C_n^1 of the neutron.

Results on the beam-helicity asymmetry are also available from the CLAS Collaboration at Jefferson Lab [27]. They are presented in Fig. 9 in comparison to results from the Hall A Collaboration and to various model calculations, in a multi-dimensional binning in x, Q^2, and t. The widely used VGG model [25], shown as curve, clearly overshoots data, which has to be kept in mind when using the model in the extraction of quark angular momentum. The situation does not change much when including contributions that are sub-leading in the twist expansion (denoted as "VGG + twist3").

All results presented so far are based on the missing-mass technique for ensuring exclusivity. For that the kinematics of the observed final-state particles (the scattered lepton and the real photon) are used to calculate the invariant mass of the missing state. The process of interest has only one proton as an additional final-state particle, thus the missing mass reconstructed should correspond to the mass of the proton. This technique is hampered by experimental resolution and leaves in general a substantial amount of background from *associated production* (excitation of the nucleon to a higher-mass state), indicated, e.g., in Fig. 6 in the bottom row as "associated fraction", as well as from semi-inclusive processes and other exclusive processes (e.g., exclusive production of neutral pions). In particular the contribution from associated production is usually not subtracted because little is known about the size of their asymmetry amplitudes.

vector meson	contribution of quarks and gluons
ρ^0	$2u+d$, $\frac{9}{4}g$
ω	$2u-d$, $\frac{3}{4}g$
ϕ	s, g
ρ^+	$u-d$
J/Ψ	g

Table 1: Quark combinations relevant in exclusive vector-meson production (see, e.g., Ref. [29])

During the last two years of data-taking, the HERMES experiment ran with a recoil-detector in place. This allowed for a complete reconstruction of the event. The resulting purity of the DVCS event sample is well above 99%, making it a unique data set among all the presently available DVCS data. This is to be compared to a fraction of associated production reaching 30% in the highest t bins at the same experiment without usage of the recoil detector.

The resulting preliminary Fourier amplitudes for the beam-helicity asymmetry are presented in Fig. 10 compared to amplitudes extracted for a reference sample in which the reconstructed momentum of the missing state X in $ep \to e\gamma X$ points into the recoil-detector acceptance [28]. The latter sample still has a large fraction of associated events. In general, the leading amplitude of the pure DVCS sample has in average a larger magnitude than the reference sample, which is diluted by associated production.

4.2. *Exclusive production of vector mesons*

Exclusive vector-meson production is a rich field for phenomenology. One complications compared to DVCS arises through the presence of an additional meson amplitude in the theoretical description (cf. Fig. 2). As mentioned in Sec. 1 at leading twist, production of vector mesons provide sensitivity only to the GPDs H^q, E^q, H^g, and E^g.

Due to the differing quark contents of the various vector mesons, one obtains also sensitivity to different quark combinations of GPDs. They are given for a few candidates in Table 1. As it turns out, the ω and the ρ^+ are particularly interesting as transverse target-spin asymmetries in exclusive vector-meson productions are expected to be large. This is due to the non-cancellation of the GPD E for the quark combinations involved assuming they have opposite signs for u and d quarks (as commonly done).

Vector mesons are also an interesting object for another reason as their decay-particle distributions reveal the polarization of the parent vector meson. This can

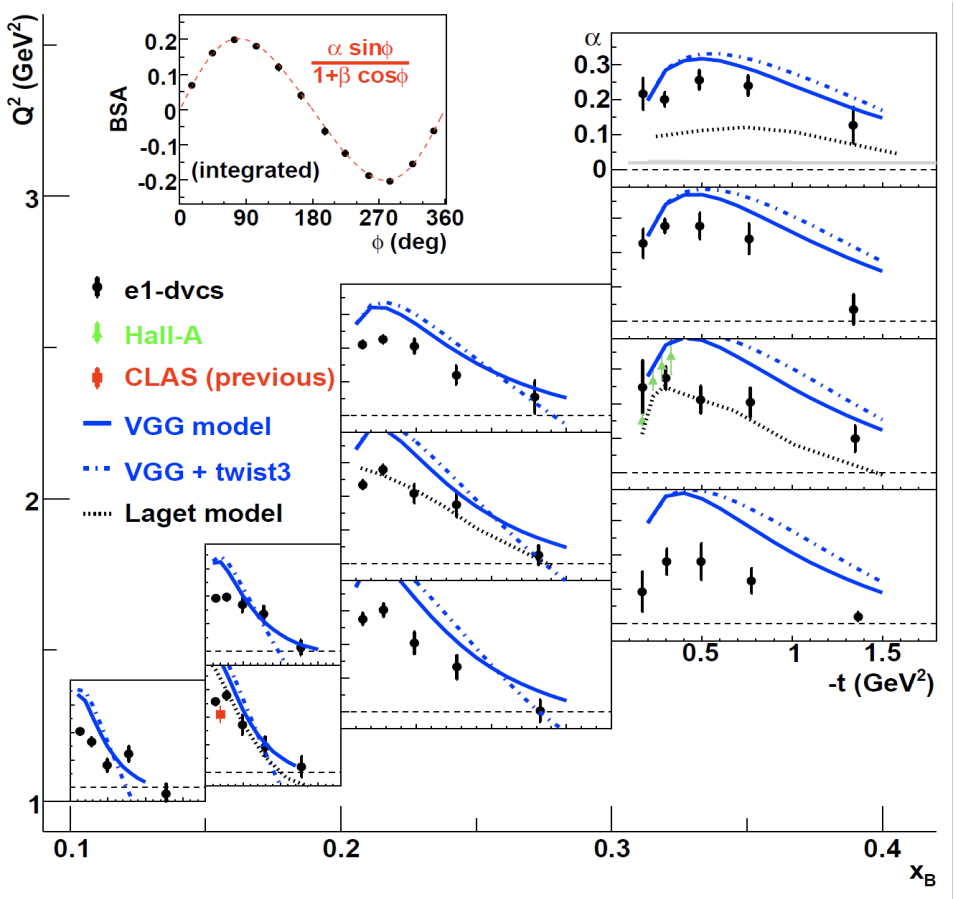

Figure 9: The leading Fourier amplitude of the beam-helicity asymmetry as measured by the CLAS Collaboration in a multi-dimensional binning in x_B, t and Q^2. The data are compared to previous results from CLAS (in the low-Q^2 bin of the second lowest x_B bin) and to data from the Hall A Collaboration (in the second lowest Q^2 bin of the highest x_B bin), as well as to model predictions denoted in the figure (see also discussion in text). The inlet describes the fit function to the ϕ dependence of the asymmetry.

be used to the study of helicity transitions from virtual photon to the vector meson. The amplitudes of the various angular dependences allow the extraction of spin-density matrix elements (SDMEs) [30, 31, 32]. They are presented in Fig. 11 for ρ^0 production on unpolarized protons or deuterons with unpolarized or longitudinally polarized beam, measured by HERMES [33, 34].

The extracted 23 SDMEs are categorized into five classes [33]: Class A comprises SDMEs dominated by the two helicity-conserving ρ^0 production amplitudes which describe the transitions $\gamma^*_L \to \rho^0_L$ and $\gamma^*_T \to \rho^0_T$, respectively. Class B contains SDMEs that correspond to the interference of the above two amplitudes. Class C and D consist of all those SDMEs involving s-channel helicity flip, corresponding to the $\gamma^*_T \to \rho^0_L$ transition, and class E involves double spin flip. As expected helicity conserving terms are much bigger in magnitude than SDMEs involving helicity-flip. However, evidence for small breaking of s-channel helicity conservation can be observed for several SDMEs of class C, D, and E.

Data on exclusive ρ^0 production comes also from the CLAS Collaboration, where the cross section has been measured to high precision on unpolarized protons [35]. A large increase in the cross section for production of longitudinal ρ^0 was observed towards low W, in a region, however, in which the handbag approach [36, 37, 38, 39, 40] of Fig. 2 may not be applicable any longer

More interesting in the context of GPDs are the SDMEs for exclusive vector-meson lepto-production on transversely polarized nucleons. One of them is sensitive to the GPD E, necessary to constrain the angular momentum of quarks and gluons [32]. The HERMES Collaboration has published results for ρ^0 production from transversely polarized protons [41]. They are shown in Fig. 13. The first SDME, related to GPD E, is

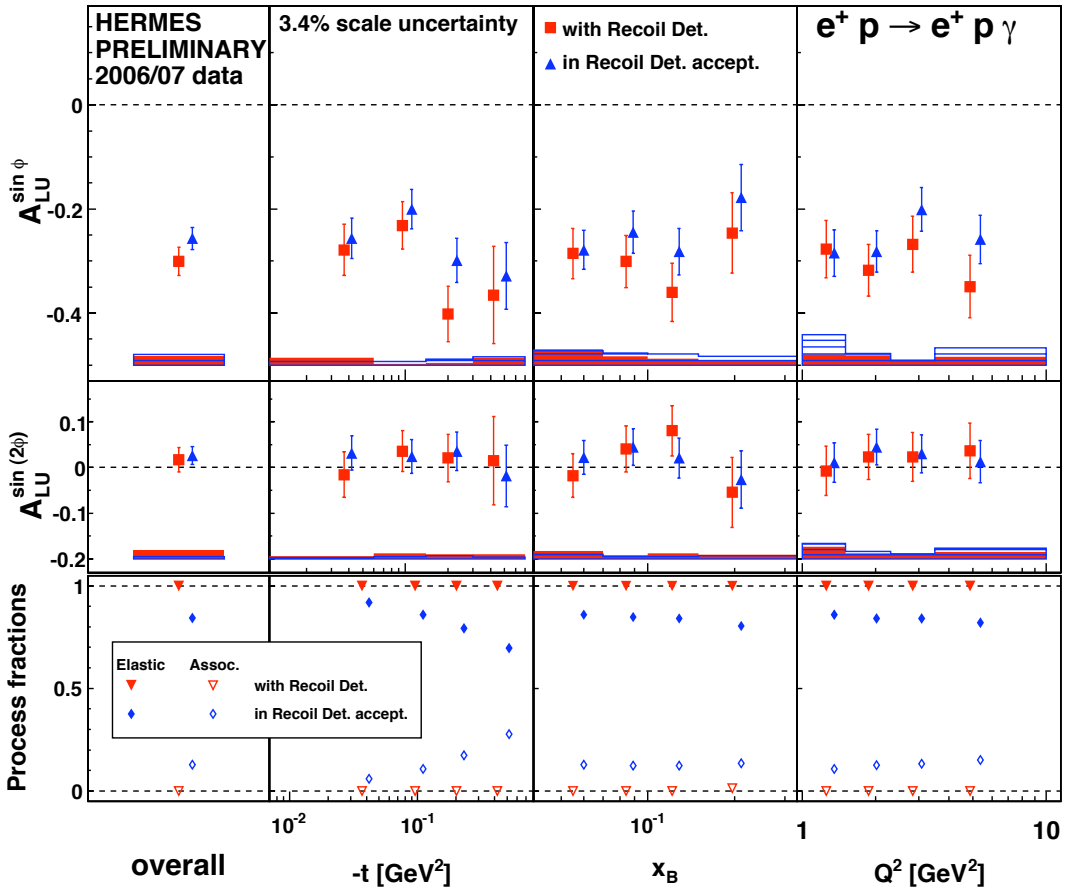

Figure 10: Results from HERMES on beam-helicity asymmetry amplitudes for a pure DVCS sample (squares), reconstructed using a recoil detector, and a reference sample (triangles) that includes a significant fraction of associated production (cf. bottom row).

consistent with zero. This was partially anticipated due to opposite signs of E^d and E^u and the particular quark-flavor combination $2u + d$ in ρ^0 production as given in Table 1, which leads to cancelations [38]. Nevertheless, these data can be used to constrain, again in a model-dependent way, the angular momentum of quarks as illustrated in Fig. 14. Also shown, in Fig. 15, are preliminary results on the same single-spin asymmetry from the COMPASS Collaboration, albeit not separated into transverse and longitudinal ρ^0 mesons. The COMPASS Collaboration has vastly increased statistics during the past years which will allow a much more precise determination of this asymmetry amplitude.

4.3. GPD phenomenology

Important progress has been achieved during the past years in GPD phenomenology. Two directions are felt to be worthwhile to be mentioned in this experimental review.[2] On one side data on exclusive meson production is used to constrain a set of GPDs [36, 37, 38, 39]. One example of this work is shown in Fig. 16.

On the other side, DVCS data is used in a global fit to constrain only the GPD H from very low values of x (using results from the HERA collider) to the kinematic regions of the fixed-target experiments [43]. Results are shown in Fig. 17, and were also discussed in more detail during this Workshop [42].

5. Outlook

Although enormous progress has been made both on theoretical and experimental side in the endeavor of determining GPDs, the situation is far from satisfactory, especially in view of the precision available for ordinary

[2] The theoretical aspects of this field are covered in a separate contribution to this Workshop [42].

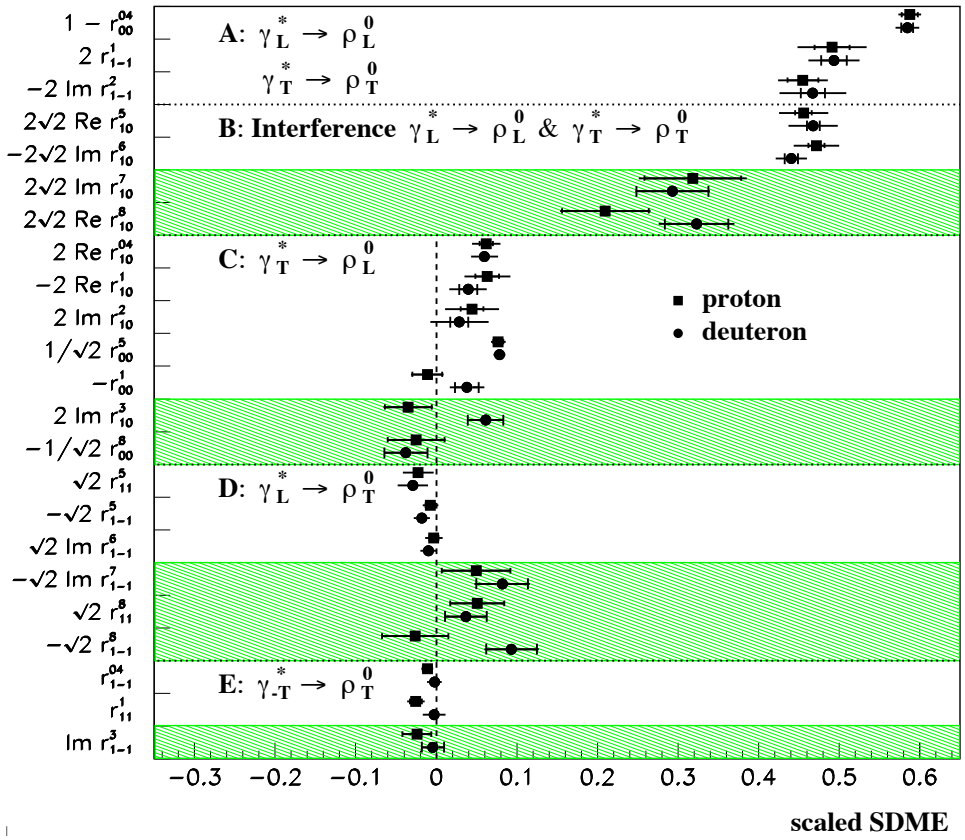

Figure 11: Results from HERMES on ρ^0 SDMEs on unpolarized protons and deuterons (see text for details).

PDFs (cf. discussion at this workshop [44]). One of the reasons is the problem that GPDs are hard to access experimentally. Using exclusive channels (vs. inclusive ones mostly entering fits of ordinary PDFs) has an immediate impact on the statistical precision achievable. It is thus not surprising that the focus is on getting data from high-luminosity experiments. In this quest, constraining the GPD H will be the easiest task (similar to the situation of ordinary PDFs, for which knowledge on the unpolarized PDFs is far advanced compared to the polarized ones).

The most intriguing GPD, however, might be at the moment the GPD E. It is needed to evaluate the decomposition of the nucleon spin via the Ji relation. Moreover, it is also linked to the *Sivers effect* [45], attributed to a naive-T-odd TMD appearing in various single-spin asymmetries with a peculiar universality property (it changes sign when going from DIS to Drell–Yan [46]) still to be verified.

Almost all experimental channels to obtain information on E involve transverse target polarization with the exception of DVCS on a neutron target (^{3}He is used as an effective neutron target that can also be polarized easily). Enormous efforts go thus into developing polarized targets allowing for large luminosities and purity. The prerequisite of reconstructing exclusive events with good resolution in all kinematic dependences leads to targets not too large in size to avoid significant smearing in kinematics due to multiple scattering. These considerations also play a role when combining the target with a recoil detector. In particular space limitations almost exclude large installations for producing and maintaining the target polarization in the target region. Therefore the focus is on polarizable targets with large relaxation times. These are foreseen both at COMPASS [47] and CLAS for measurements of the GPD E. The COMPASS Collaboration has as well a program to measure exclusive reactions constraining GPD H, for which target polarization is not a requirement.

Data taking at the Jefferson Lab experiments will stop in 2012 to start the upgrade of the accelerator to a beam energy of 12 GeV, and also of the detectors in the various experimental halls. This upgrade is scheduled to be finished by summer of 2015. While CLAS12 will be

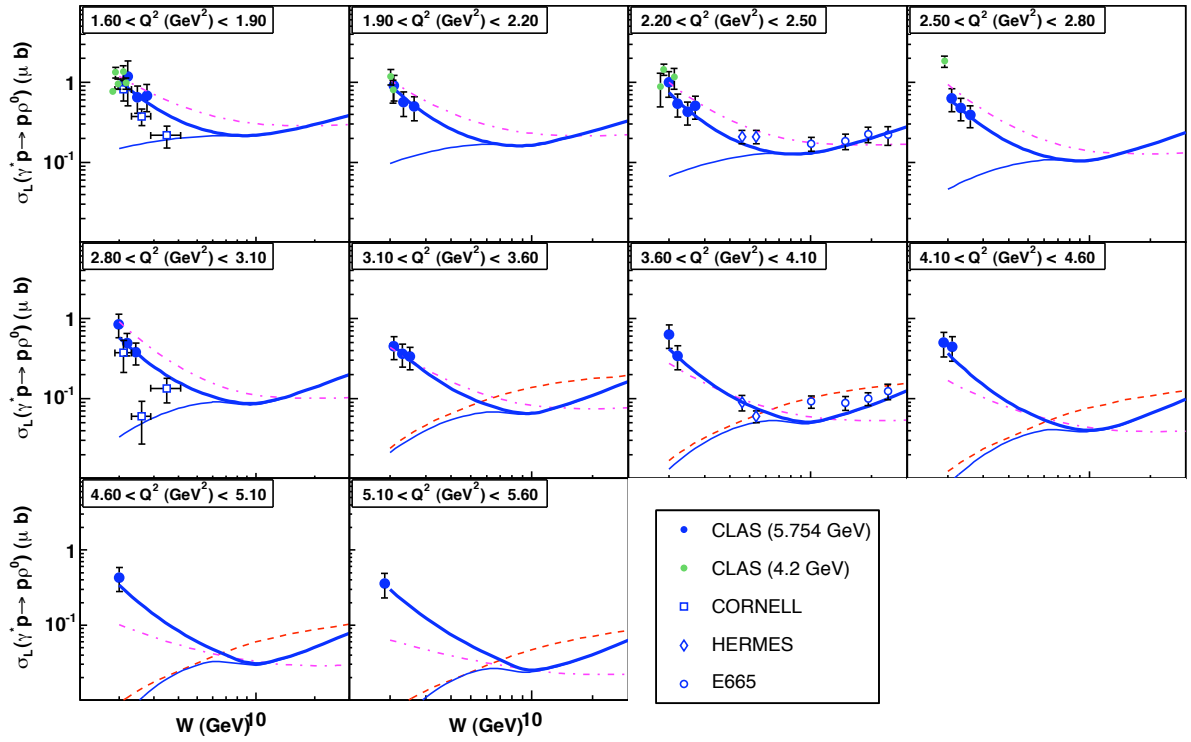

Figure 12: World data for the reduced cross sections $\gamma^*_L p \to \rho^0_L p$ as a function of W for constant Q^2 bins, overlaid with various model calculations. The dashed curve shows the result of the calculations by Goloskokov and Kroll [36] and the thin solid curve shows the result of the VGG model. The thick solid curve is a modified VGG calculation, while the dot-dashed curve shows the results of a Regge-Ansatz calculation.

the major facility for DVCS cross sections and beam-/target-polarization related observables, high-statistics data are also to be expected from the Hall-A spectrometer, albeit in a reduced kinematic regime.

The most ambitious program to date is likely the proposed electron-ion-collider (EIC) [48]. It would allow with unprecedented luminosity over a large kinematic range and combinations of beam and target polarizations a detailed mapping of GPDs. Two competing designs, one at Jefferson Lab and one at Brookhaven National Laboratory, are under discussion. The high luminosities envisaged would allow another channel not discussed so far: double deeply virtual Compton scattering (DDVCS), the exclusive lepto-production of virtual photons (leading, e.g., to a lepton pair in the final state). Unlike DVCS, which provide information on GPDs along the diagonal $x = \xi$ or their x-integral only, DDVCS has the potential to map the whole kinematic space on which GPDs depend upon.

The kinematic range and luminosity of an future EIC would also provide the possibility to study in detail the Q^2 dependence of DVCS. It has been shown that this has the potential to access GPD's kinematic dependences beyond the usual limitations [48].

6. Summary

The past decade marks the beginning of the exploration of GPDs via exclusive lepto-production of either real photons or mesons. Progress has been largest in constraining the GPD H, which is easiest to study as it does not require transverse target polarization. The latter is needed for measurements of observables that have a significant sensitivity to the GPD E when using a proton target (an unpolarized neutron target has been demonstrated to allow access to the GPD E). So far such measurements exist only from the decommissioned HERMES experiment. It is thus of utterly importance to work on transverse-target programs. Indeed, both the COMPASS and the Jefferson Lab collaborations are planning future measurements of exclusive reactions with transversely polarized protons. A completely new dimension in the analysis of GPDs would be provided by a future EIC. Its luminosity and kinematic range would allow the complete kinematic mapping of the GPD H and E, possibly testing the Ji relation, but also of many of the other GPDs.

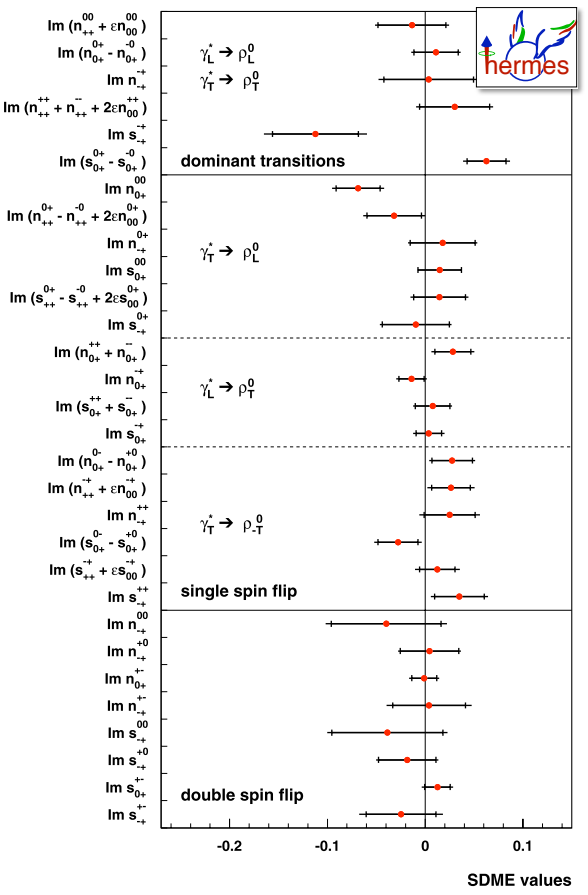

Figure 13: HERMES results on ρ^0 SDMEs for transversely polarized protons. The top one, corresponding to $\mathrm{Im}(n^{00}_{++} + \epsilon n^{00}_{00})$, involves the GPD E.

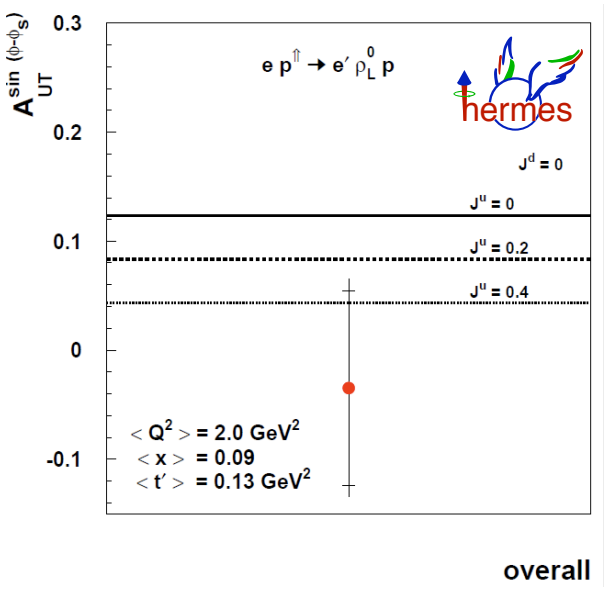

Figure 14: Transverse single-spin asymmetry for longitudinal ρ^0 mesons produced on transversely polarized protons at HERMES, as derived from the SDMEs for transversely polarized protons. Also shown are model curves based on GPD models with the angular momentum of u and d quarks as parameters.

To conclude, despite the vast difficulties both on the experimental but also phenomenological sides great advances have been achieved in the study of the GPD H. While some results provide important constraints on the GPD E, much more precision is needed to reach a level in understanding that would allow, e.g., the evaluation of the Ji relation and thus results on the angular momentum carried by quarks. This exploration will be part of the experimental programs at COMPASS and the Jefferson Lab experiments after the 12 GeV upgrade, as well as at a future EIC.

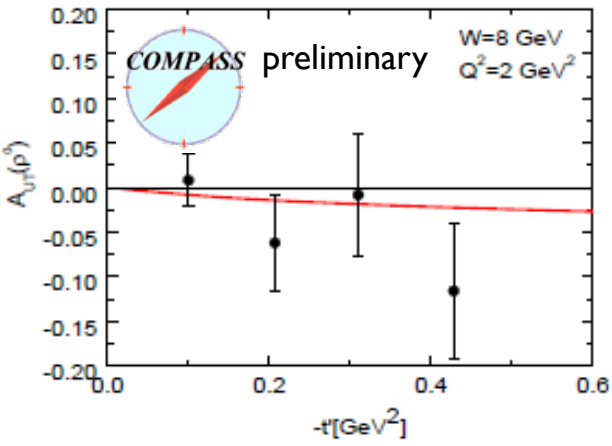

Figure 15: Transverse single-spin asymmetry for longitudinal and transverse ρ^0 mesons combined, produced on transversely polarized protons at COMPASS.

7. Acknowledgements

This work was partially funded by the Basque Foundation for Science, IKERBASQUE.

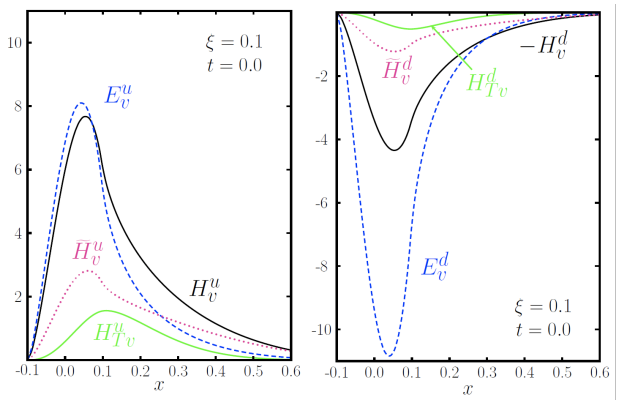

Figure 16: Various valence-quark GPDs vs. x at $\xi = 0.1$ and $t = 0$ (at a scale of $Q^2 = 4$ GeV^2) extracted from fits to data on exclusive meson production.

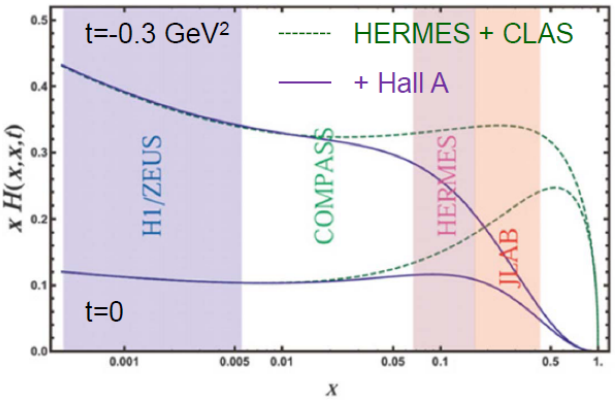

Figure 17: A global fit of GPD H to world data for $t = 0$ and $t = 0.3$ GeV^2. The difference between the two curves in both cases are the inclusion of the data by the Hall A collaboration (solid line).

References

[1] D. Müller *et al.*, Fortschr. Phys. 42 (1994) 101.
[2] A. V. Radyushkin, Phys. Lett. B380 (1996) 417. [hep-ph/9604317].
[3] A. V. Radyushkin, Phys. Rev. D56 (1997) 5524. [hep-ph/9704207].
[4] X. Ji, Phys. Rev. Lett. 78 (1997) 610613. [hep-ph/9603249].
[5] M. Burkardt, Phys. Rev. D62 (2000) 071503; Erratum–ibid. D66 (2002) 119903. [hep-ph/0005108].
[6] M. Diehl, Eur. Phys. J. C25 (2002) 223; Erratum-ibid. C31 (2003) 277. [hep-ph/0205208].
[7] J. P. Ralston and B. Pire, Phys. Rev. D66 (2002) 111501. [hep-ph/0110075].
[8] A. V. Belitsky and D. Müller, Nucl. Phys. A711 (2002) 118. [hep-ph/0206306].
[9] M. Burkardt, Int. J. Mod. Phys. A18 (2003) 173. [hep-ph/0207047].
[10] J. C. Collins and A. Freund, Phys. Rev. D59 (1999) 074009. [hep-ph/9801262].
[11] A. V. Belitsky, D. Müller and A. Kirchner, Nucl. Phys. B629 (2002) 323-392. [hep-ph/0112108].
[12] J. C. Collins, L. Frankfurt, and M. Strikman, Phys. Rev. D56 (1997) 2982. [hep-ph/9611433].
[13] A. V. Radyushkin, Phys. Lett. B385 (1996) 333. [hep-ph/9605431].
[14] A. Bacchetta, U. D'Alesio, M. Diehl, and C. A. Miller, Phys. Rev. D70 (2004) 117504. [hep-ph/0410050].
[15] S. Stepanyan *et al.* [CLAS Collaboration], Phys. Rev. Lett. 87 (2001) 182002. [hep-ex/0107043].
[16] A. Airapetian *et al.* [HERMES Collaboration], Phys. Rev. Lett. 87 (2001) 182001. [hep-ex/0106068].
[17] A. Airapetian *et al.* [HERMES Collaboration], JHEP 11 (2009) 083. [arXiv:0909.3587 [hep-ex]].
[18] A. Airapetian *et al.* [HERMES Collaboration], Nucl. Phys. B829 (2010) 1. [arXiv:0911.0095 [hep-ex]]
[19] A. Airapetian *et al.*, [HERMES Collaboration], JHEP 06 (2008) 066. [arXiv:0802.2499 [hep-ex]]
[20] A. Airapetian *et al.*, [HERMES Collaboration], Phys. Lett. B704 (2011) 15. [arXiv:1106.2990 [hep-ex]]
[21] A. Airapetian *et al.*, [HERMES Collaboration], JHEP 06 (2010) 019. [arXiv:1004.0177 [hep-ex]]
[22] A. Airapetian *et al.*, [HERMES Collaboration], Nucl. Phys. B842 (2011) 265. [arXiv:1008.3996 [hep-ex]]
[23] V. Burkert, presented at Transversity 2011 (2011).
[24] M. Mazouz *et al.*, [Jefferson Lab Hall A Collaboration], Phys. Rev. Lett. 99 (2007) 242501. [arXiv:0709.0450 [nucl-ex]].
[25] M. Vanderhaeghen, P.A.M. Guichon, and M. Guidal, Phys. Rev. D60 (1999) 094017. [hep-ph/9905372].
[26] S. Ahmad, H. Honkanen, S. Liuti, S. K. Taneja, Phys. Rev. D75 (2007) 094003. [hep-ph/0708.0268].
[27] F. Girod *et al.* [CLAS Collaboration], Phys. Rev. Lett. 100 (2008) 162002. [arXiv:0711.4805 [hep-ex]].
[28] S. Yaschenko *et al.*, [HERMES Collaboration], DIS 2011 proceedings (2011).
[29] M. Strikman and C. Weiss, arXiv:0804.0456 [hep-ph].
[30] K. Schilling and G. Wolf, Nucl. Phys. B61 (1973) 381.
[31] H. Fraas, Ann. Phys. 87 (1974) 417.
[32] M. Diehl, JHEP 09 (2007) 064. [arXiv:0704.1565 [hep-ph]].
[33] A. Airapetian *et al.* [HERMES Collaboration], Eur. Phys. J. C62 (2009) 659. [arXiv:0901.0701 [hep-ex]].
[34] A. Airapetian *et al.* [HERMES Collaboration], Eur. Phys. J. C71 (2011) 1609. [arXiv:1012.3676 [hep-ex]].
[35] S. A. Morrow *et al.* [CLAS Collaboration], Eur. Phys. J. bf A39 (2009) 5. [arXiv:0807.3834 [hep-ex]]
[36] S. V. Goloskokov and P. Kroll, Eur. Phys. J. C42 (2005) 281. [arXiv:hep-ph/0501242].
[37] S. V. Goloskokov and P. Kroll, Eur. Phys. J. C53 (2008) 367. [arXiv:0708.3569v2 [hep-ph]].
[38] S. V. Goloskokov and P. Kroll, Eur. Phys. J. C59 (2009) 809. [arXiv:0809.4126 [hep-ph]].
[39] S. V. Goloskokov and P. Kroll, Eur. Phys. J. C65 (2010) 137. [arXiv:0906.0460 [hep-ph]].
[40] P. Kroll, AIP Conf. Proc. 1374 (2011) 103. [arXiv:1009.2356 [hep-ph]].
[41] A. Airapetian *et al.* [HERMES Collaboration], Phys. Lett. B679, 100 (2009). [arXiv:0906.5160 [hep-ex]].
[42] K. Kumericki, these proceedings.
[43] K. Kumericki and D. Müller, Nucl. Phys. B841 (2010) 1. [arXiv:0904.0458 [hep-ph]].
[44] K. Lipka, these proceedings.
[45] D. W. Sivers, Phys. Rev. D41 (1990) 83.
[46] J. C. Collins, Phys. Lett. B536 (2002) 43. [hep-ph/0204004]
[47] The COMPASS Collaboration, CERN–SPSC–2010–014, http://wwwcompass.cern.ch/compass/proposal/compass-II_proposal/compass-II_proposal.pdf
[48] D. Boer *et al.* [arXiv:1108.1713 [nucl-th]].